PHARMACIA

Pharmacia 71: 1–19
DOI 10.3897/pharmacia.71.e123948

Research Article

Molecular docking-based virtual screening and computational investigations of biomolecules (curcumin analogs) as potential lead inhibitors for SARS-CoV-2 papain-like protease

Taufik Muhammad Fakih[1,2], Ritmaleni[3,4], Rahadian Zainul[5], Muchtaridi Muchtaridi[1,6]

1 *Department of Pharmaceutical Analysis and Medicinal Chemistry, Faculty of Pharmacy, Universitas Padjadjaran, Jl. Raya Bandung Sumedang KM 21, Sumedang, 45363, Indonesia*
2 *Department of Pharmacy, Faculty of Mathematics and Natural Sciences, Universitas Islam Bandung, Jl. Ranggagading, Bandung, 40116, Indonesia*
3 *Laboratory of Medicinal Chemistry, Department of Pharmaceutical Chemistry, Faculty of Pharmacy, Universitas Gadjah Mada, Jl. Sekip Utara, Yogyakarta, 55281, Indonesia*
4 *Curcumin Research Center, Faculty of Pharmacy, Universitas Gadjah Mada, Jl. Sekip Utara, Yogyakarta, 55281, Indonesia*
5 *Department of Chemistry, Faculty of Mathematics and Natural Sciences, Universitas Negeri Padang, Jl. Prof Dr Hamka Kampus Air Tawar, Padang, 25131, Indonesia*
6 *Research Collaboration Centre for Theranostic Radio Pharmaceuticals, National Research and Innovation Agency (BRIN), Jl. Raya Bandung Sumedang KM 21, Sumedang, 45363, Indonesia*

Corresponding author: Muchtaridi Muchtaridi (muchtaridi@unpad.ac.id)

Received 25 March 2024 ♦ **Accepted** 1 May 2024 ♦ **Published** 25 June 2024

Citation: Fakih TM, Ritmaleni, Zainul R, Muchtaridi M (2024) Molecular docking-based virtual screening and computational investigations of biomolecules (curcumin analogs) as potential lead inhibitors for SARS-CoV-2 papain-like protease. Pharmacia 71: 1–19. https://doi.org/10.3897/pharmacia.71.e123948

Abstract

In the effort to combat SARS-CoV-2 infection, researchers are currently exploring the repurposing of conventional antiviral drugs, despite their limited efficacy. The SARS-CoV-2 virus encodes a papain-like protease (PLpro), which not only plays a crucial role in viral replication but also cleaves ubiquitin and interferon-stimulated gene 15 protein (ISG15) from host proteins, making it a prime target for the development of new antiviral medications. In this study, we conducted a multi-step in silico screening to identify novel, noncovalent PLpro inhibitors. Curcumin, an antioxidant derived from turmeric rhizomes (Curcuma longa L.), has undergone extensive preclinical investigations and shown significant efficacy against viruses and other ailments in both laboratory and animal studies. However, the pharmacological limitations of curcumin have prompted the synthesis of numerous novel curcumin analogs, necessitating evaluation for their therapeutic potential. The selectivity of the top-scoring compounds was assessed through molecular docking studies and molecular dynamics simulations to determine their binding affinity to PLpro. As a result, we identified 20 potential, selective PLpro inhibitors, from which the top two compounds (THA111 and THHGV6) were selected based on their binding free energy values towards PLpro as estimated by MM-PBSA calculations. These selected candidates demonstrate promising activity against the protein, with binding free energy values ranging from approximately −105 to −108 kJ/mol, and largely adopt a similar binding mode to known noncovalent SARS-CoV-2 PLpro inhibitors (GRL0617 = −100.98 kJ/mol). We further propose these two most promising compounds for future in vitro evaluation. The findings for the top potential PLpro inhibitors have been deposited in a database (Curcumin Research Center) to aid research on anti-SARS-CoV-2 drugs.

Keywords

SARS-CoV-2 PLpro, Curcumin analogs, COVID-19 therapy, Virtual drug screening, Computational investigations

Introduction

Due to the rapid and widespread transmission rates, the World Health Organization (WHO) officially classified coronavirus disease 2019 (COVID-19) as a global health emergency and declared it a pandemic on March 11, 2020 (Kong et al. 2021). Severe acute respiratory syndrome coronavirus 2 (SARS-CoV-2) was identified as the causative agent of COVID-19 (Gil et al. 2020). Individuals infected with SARS-CoV-2 may exhibit mild symptoms such as fever, cough, and fatigue, but the virus can also lead to severe respiratory complications, organ failure, and death. Elderly individuals and those with underlying health conditions are particularly vulnerable to experiencing a severe course of the illness (Wurtzer et al. 2020; Fernández-Castañeda et al. 2022). As of March 2021, the global death toll from COVID-19 has surpassed 2.5 million, with more than 114 million confirmed cases reported worldwide (Abduljalil and Abduljalil 2020). Given its significant impact on public health and its profound socio-economic ramifications, the scientific community has dedicated substantial efforts to the development of novel treatments.

SARS-CoV-2 belongs to the Coronaviridae family and is an enveloped positive-sense RNA virus (Cheung et al. 2021). During the infection process, viral polypeptides (pp1a and pp1ab) are synthesized and require proteolytic cleavage by specific enzymes to become functional peptides. In SARS-CoV-2, papain-like protease (PLpro) has been identified as essential for this cleavage process (Li et al. 2021; Tan et al. 2022). Since this protease plays a crucial role in viral replication, it emerges as a promising target for drug development. Inhibiting viral proteases involved in polypeptide processing has proven to be an effective strategy for treating other viral infections, such as hepatitis C virus (HCV) and human immunodeficiency virus (HIV) (Bianchi and Pessi 2002; Hulce et al. 2022).

The SARS-CoV-2 PLpro enzyme plays a crucial role in viral replication and in dampening the host immune response, making it an attractive target for intervention (Zhao et al. 2022). Consequently, it has garnered significant attention from the scientific community, leading to investigations into its structure, functions, and comparisons with PLpro enzymes from related coronaviruses, particularly SARS-CoV (Yapasert et al. 2021). Efforts to identify PLpro inhibitors are already underway, with current studies primarily focusing on adapting existing noncovalent inhibitors developed for SARS-CoV or designing specific covalent inhibitors (van Vliet et al. 2022). However, the latter approach carries risks of toxicity due to high reactivity and potential off-target binding. In light of this, there is a growing interest in developing noncovalent PLpro inhibitors, leveraging existing data on SARS-CoV PLpro inhibitors to inform the design of analogous inhibitors for SARS-CoV-2 (Osipiuk et al. 2021; Sencanski et al. 2022). Despite recent efforts, the binding affinities of newly developed SARS-CoV-2 PLpro inhibitors remain moderate. Therefore, there is a pressing need for a more comprehensive approach to design novel PLpro inhibitors with enhanced binding affinities and reduced toxicity risks.

At present, numerous researchers have indicated the potential of plant-derived chemical compounds in combating SARS-CoV-2 infection, which could potentially prevent the onset or severity of COVID-19. Among these compounds, curcumin, the primary polyphenolic component found in turmeric, has garnered considerable attention due to its diverse biological effects, including its anti-tumor, anti-inflammatory, immunomodulatory, antioxidant, and antimicrobial properties (Zorofchian Moghadamtousi et al. 2014; Urošević et al. 2022). Moreover, curcumin has demonstrated inhibitory effects against the replication of various viruses, including dengue virus, hepatitis B virus, zika virus, influenza A virus, and chikungunya virus (Adamczak et al. 2020). Its antiviral actions can target the viral particle directly or interfere with different stages of the viral replication cycle by interacting with viral proteins or modulating critical cellular processes and pathways necessary for viral replication (Sun et al. 2010; Kotha and Luthria 2019).

Interestingly, previous in vitro studies have shown that post-infection treatment with curcumin at a concentration of 10 μg/mL exhibits significant antiviral effects against SARS-CoV-2, with inhibition rates of 99% and 99.8% against the DG614 strain and Delta variant respectively (Marín-Palma et al. 2021). Another study also demonstrated that administration of curcumin at a concentration of 10 μM to the virus before inoculation into cell culture resulted in inhibition of SARS-CoV-2 replication, with a reduction rate of over 99% in Vero E6 cells (Zupin et al. 2022). Additionally, several recent molecular docking studies have suggested that curcumin may inhibit the viral protein translation process by interacting with the active sites of the 3CLPro and PLPro enzymes (Linda Laksmiani et al. 2020; Das et al. 2021). Thus, specifically concerning SARS-CoV-2, computational modeling studies have indicated that curcumin shows promising binding affinities with the PLPro.

In this study, we aimed to discover new, potent, noncovalent, and specific inhibitors of PLpro. These compounds are anticipated to exhibit greater binding affinity to SARS-CoV-2 PLpro compared to existing inhibitors. To accomplish this objective, we conducted thorough in silico screening, a modern and efficient approach in drug design. We placed a strong emphasis on the accuracy of our predictions by extensively validating the techniques utilized to ensure their applicability to our project. Consequently, we employed a variety of computational methods, merging both ligand-based and structure-based strategies. Initially, our focus was on curcumin analogs, comprising a total of 20 compounds synthesized successfully in our laboratory. Subsequently, we assessed the binding affinities of selected molecules to SARS-CoV-2 PLpro through molecular docking and molecular dynamics simulations. These findings have been archived in a publicly accessible database to facilitate future research endeavors aimed at combating the COVID-19 pandemic.

Materials and methods

Preparation and optimization of curcumin analogs

The structural configurations of the compounds intended for the study were derived from both two-dimensional and three-dimensional representations generated using ChemDraw Professional 16.0 and Chem3D 16.0 software (Brown 2014). Subsequently, these structures underwent optimization procedures using GaussView 6.0 and Gaussian16 software, employing various parameters such as Density Functional Theory (DFT) or Hartree-Fock calculation methods, 3-21G basis sets, and simulation conditions under vacuum (Frisch et al. 2009). The optimization process yielded data on the geometry of the compounds, including their energy stability, electron distribution, and reactive conformations. This structural optimization aimed to attain a stable conformation suitable for physiological conditions, accomplished by incorporating polar hydrogen atoms and calculating Gasteiger charges (Fakih 2023).

Preparation of SARS-CoV-2 papain-like protease (PLpro) macromolecules

The three-dimensional configuration of the SARS-CoV-2 papain-like protease (PLpro) receptor macromolecule was acquired from the Protein Data Bank (PDB) website via the URL https://www.rcsb.org/structure/3e9s (Ratia et al. 2008). Afterwards, the structure underwent preparation procedures using the Discovery Studio 2019 Client to eliminate undesirable components such as native ligands (GRL0617), water and solvent molecules, and irregular elements (BIOVIA 2017). This preparation aimed to generate a refined structure in accordance with specified conditions, achieved by adding polar hydrogen atoms and computing Kollman charges. These steps were taken to establish a stable structure suitable for molecular docking and molecular dynamics simulations. Following this, the identification of active binding sites was conducted to pinpoint locations where the compound could potentially bind to the receptor. Active binding sites were identified by assessing their potential and evaluating the interactions between these sites and the compounds (Nurisyah et al. 2024).

Molecular docking studies

Molecular docking investigations of curcumin derivative compounds against SARS-CoV-2 PLpro macromolecules were conducted using AutoDock 4.2 to explore potential interactions between these curcumin analog compounds and SARS-CoV-2 PLpro macromolecules (Forli et al. 2012). The molecular docking studies employed a grid box measuring 64 × 60 × 60 points with a spacing of 0.375 Å to encompass the binding site of the target. The Lamarckian Genetic Algorithm (LGA) was utilized with 100 conformations for each simulation, while other docking parameters were kept at default settings (Forli et al. 2012). LGA, an optimization technique employed in AutoDock 4.2, aimed to determine the optimal conformation of curcumin analog compounds binding to receptor proteins. This algorithm seeks to optimize the interaction energy between curcumin analog compounds and receptor proteins by identifying the most stable conformation through a combination of mutation and crossover.

ADMET properties of curcumin analogs

The pharmacological and pharmacokinetic characteristics of all curcumin derivative compounds were assessed through the SwissADME (Daina et al. 2017) and pkCSM (Pires et al. 2015) online platforms. These tools analyze the input structure against a set of data and predict various properties based on specific parameters. The SwissADME and pkCSM webservers compare the input structure with the training set and calculate the probable properties based on different parameters, providing valuable insights for drug development and optimization.

PASS identification of curcumin analogs

The PASS website was employed for forecasting the pharmacological and biological traits of the substances (Lohidashan et al. 2018). It scrutinizes a compound's biological potential by examining its structure-activity relationship. By comparing the desired structure with a pre-existing training set encompassing diverse biological functions, the server anticipates potential biological activities using the ratio of 'probability of being active (Pa)' to 'probability of being passive (Pi)'. A higher Pa value suggests a greater likelihood of a chemical possessing the investigated biological characteristic.

Molecular dynamics simulations

Molecular dynamics simulations lasting 100 ns were conducted utilizing Gromacs 2016.3 with the AMBER99SB-ILDN force field, which enhances the accuracy of MD simulations by incorporating the Improved Lipophilic Efficiency Descriptors for Nucleic Acids (ILDN) parameter for nucleic acids (Aragones et al. 2013; Abraham et al. 2015; Smith et al. 2015). The parameterization of curcumin analog compounds was executed using the AnteChamber PYthon Parser interface (ACPYPE) to generate the necessary input files for molecular dynamics simulations (Aragones et al. 2013; Abraham et al. 2015; Smith et al. 2015). Electrostatic forces were calculated using the Particle Mesh Ewald (PME) method, which divides the electric potential formed by charged particles into two components: the potential from nearby charged particles and the potential from distant charged particles (Ramadhan et al. 2022). System neutralization was achieved by introducing sodium (Na+) and chloride (Cl-) ions around the receptor-ligand complex. Solvation was performed using the Transferable Intermolecular Potentials 3-Point (TIP3P) water model, which defines the hydrogen, oxygen, and hydrogen bond interactions between atoms in a water molecule.

Binding free energy MM-PBSA calculation

The Molecular Mechanics-Poisson-Boltzmann Surface Area (MM-PBSA) calculations were conducted using the g_mmpbsa package, which is integrated into the Gromacs 2016.3 software (Wang et al. 2018; Mishra et al. 2022). Energy computations involved averaging data from 100 snapshots, extracted at ten ps intervals, covering the molecular dynamics trajectory from 0 to 100 ns. To calculate polar desolvation energy, the Poisson–Boltzmann equation was applied with a grid size set to 0.5 Å. The dielectric constant for the solvent was set to 80, representing water. Nonpolar energy contributions were assessed by analyzing the solvent-accessible surface area with a solvent radius of 1.4 Å. A comprehensive evaluation of receptor-ligand free energy was conducted based on stable interactions observed within the complex during molecular dynamics simulations.

Results and discussion

Molecular docking studies

The initial stage involves conducting molecular docking simulations between curcumin analogs and SARS-CoV-2 papain-like protease (PLpro) macromolecules using AutoDock 4.2 equipped with the Lamarckian Genetic Algorithm (LGA). Molecular docking serves as a computational approach to elucidate the interactions between a specific chemical compound (ligand) and a protein (target) (Ariyanto et al. 2023). The objective of this docking simulation is to identify the most stable protein-ligand complex that may occur under physiological conditions. This process entails a systematic exploration of all feasible orientations and placements of the ligands within the active site of the protein, followed by an assessment of the energy associated with each resultant complex. Various methods are employed for energy calculations, including empirical, physicochemical, and hybrid methods (Kumar et al. 2023). These energy calculations quantify the interactions among the atoms involved in the complexes, encompassing hydrogen bonds, van der Waals forces, and electrostatic interactions.

The outcomes of molecular docking investigations reveal that all curcumin analog compounds exhibit favorable affinity towards SARS-CoV-2 PLpro macromolecules. However, only five derivative compounds, namely A108, A113, A146, THA113, and THA146, demonstrate superior affinity compared to native ligands (GRL0617) (Table 1). Simulation findings indicate that these five compounds exhibit relatively high affinity and effectively bind to the active site of SARS-CoV-2 PLpro macromolecules. Detailed structural analysis of the compound-receptor complexes reveals that the five curcumin analog compounds engage with the active site of SARS-CoV-2 PLpro through hydrogen bonding and van der Waals interactions. This observation suggests that these five compounds can establish stable and efficient binding with SARS-CoV-2 PLpro. Based on the docking study results, these compounds hold promise as candidates for the development of new COVID-19 drugs. However, further assessment using molecular dynamics simulations is imperative to confirm the stability of the interaction.

In Fig. 1, the molecular interactions between SARS-CoV-2 PLpro macromolecules and curcumin analog compounds are primarily characterized by multiple hydrogen bonds and hydrophobic interactions. The analog compounds derived from curcumin, particularly A108, A113, A146, THA113, and THA146, exhibit notable interactions with amino acid residues LYS159, GLU163, LEU164, ASP166, GLU169, TYR266, THR303, and ASP304, as depicted in the figure. Notably, compounds A113 and THA113 are surrounded by numerous amino acid residues, likely attributed to the presence of a bromide (Br) atom in their molecular structure. In molecular docking studies, compounds containing such atoms tend to attract amino acid residues due to the electronegativity of bromide, resulting in a partial negative charge around the bromide atom and a partial positive charge around the bonded atom (Misran et al. 2020; Mohamed Thamby et al. 2023). Consequently, amino acid residues with a positive charge may interact with the partial negative charge induced by the bromide atom.

It's intriguing that having two symmetrically linked 1,3-dicarbonyl or α, β unsaturated carbonyl units facilitates binding with DNA, protein sites, and metals through a well-established process known as keto-enol tautomerism (Nocito et al. 2021). Additionally, the conversion from the keto to the enol form of curcumin heavily relies on the polarity of the system, making it adept at overcoming diverse barriers during biochemical processes (Shah et al. 2022). Another critical structural aspect of curcumin is its hydrophobic aromatic unit with hydroxyl and methoxy substitutions, which also significantly contribute to enhancing curcumin's efflux action (Deshmukh et al. 2020). With two hydroxyl groups present, curcumin can also serve as a potent antioxidant. While curcumin is utilized for treating various ailments (Fig. 2), exploring its antiviral potential against SARS-CoV-2 further adds to its intrigue.

ADMET properties of curcumin analogs

Physiological and pharmacokinetic traits play a critical role in the selection and advancement of drug-like substances. Compounds that successfully undergo screening for physicochemical and ADMET properties stand a better chance of achieving clinical success. The pkCSM platform computes physicochemical and ADMET parameters for all compounds chosen through docking screening. For every curcumin derivative compound, a range of ADMET parameters is evaluated concurrently with PAINS screening. This process identifies twenty compounds possessing outstanding physicochemical characteristics and devoid of any PAINS patterns (Angamuthu et al. 2019). The ADMET characteristics derived from this selection are detailed in Table 2. These chosen compounds demonstrate favorable ADMET attributes, as indicated by the absence of AMES toxicity in the pkCSM forecast.

Table 1. The free energy of binding between curcumin analogs and SARS-CoV-2 PLpro macromolecules.

Compound Molecule	Molecular Structure	Binding Free Energy
Native (GRL0617)	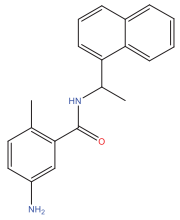	−10.05 kcal/mol
A102	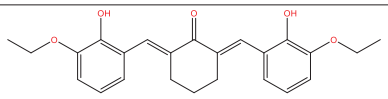	−8.01 kcal/mol
A103	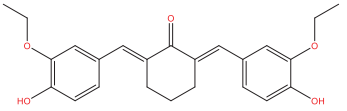	−7.27 kcal/mol
A104	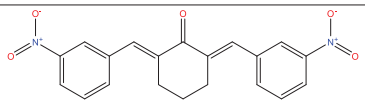	−8.57 kcal/mol
A108	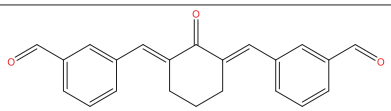	−9.22 kcal/mol
A111	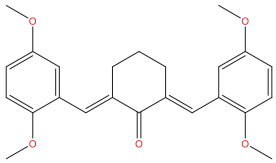	−7.90 kcal/mol
A113	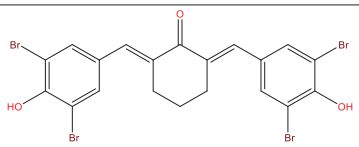	−9.85 kcal/mol
A129	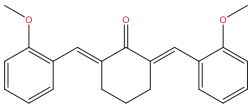	−8.52 kcal/mol
A146	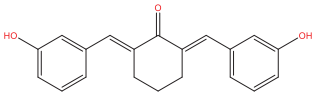	−9.96 kcal/mol
HGV5	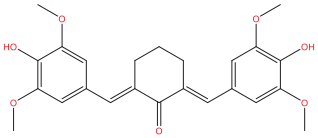	−8.18 kcal/mol
HGV6	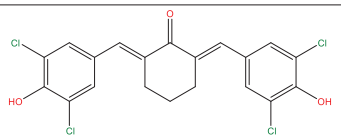	−8.65 kcal/mol
THA102	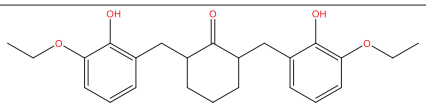	−7.83 kcal/mol
THA103	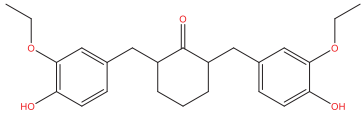	−7.61 kcal/mol
THA104	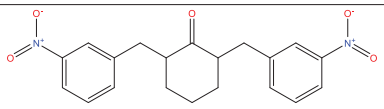	−8.83 kcal/mol

Compound Molecule	Molecular Structure	Binding Free Energy
THA108	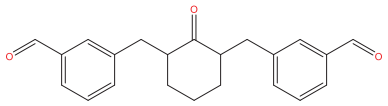	−8.89 kcal/mol
THA111	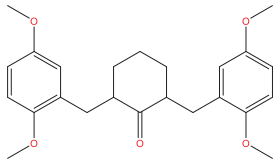	−7.15 kcal/mol
THA113	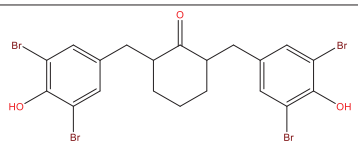	−9.29 kcal/mol
THA129	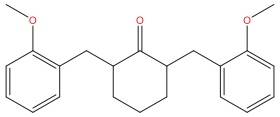	−8.14 kcal/mol
THA146	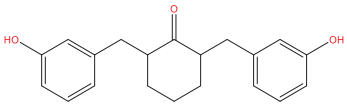	−9.56 kcal/mol
THHGV5	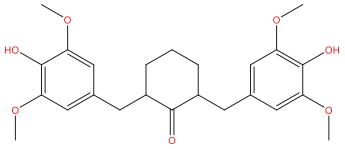	−7.47 kcal/mol
THHGV6	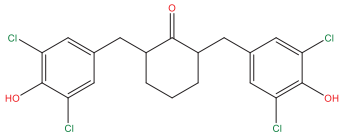	−8.93 kcal/mol

Table 2. The ADMET criteria of the curcumin analogs utilizing the pkCSM Web tool.

Compound Molecule	Molecular Structure	GI Absorption	Water Solubility (log mol/L)	BBB Permeability (log BB)	CYP2D6 Inhibitor	Renal OCT2 Substrate	AMES Toxicity
A102	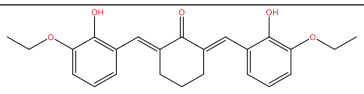	High	−3.91	Yes	Yes	No	No
A103	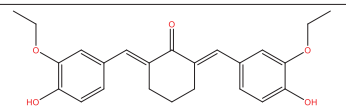	High	−3.91	Yes	Yes	No	No
A104	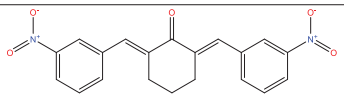	High	−4.75	No	No	No	No
A108	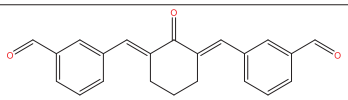	High	−4.31	Yes	Yes	No	No
A111	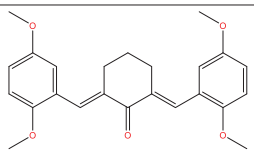	High	−4.13	Yes	Yes	No	No
A113	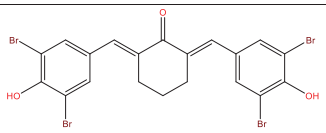	High	−5.76	No	No	No	No

Compound Molecule	Molecular Structure	GI Absorption	Water Solubility (log mol/L)	BBB Permeability (log BB)	CYP2D6 Inhibitor	Renal OCT2 Substrate	AMES Toxicity
A129	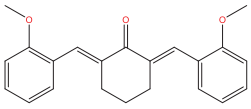	High	−4.67	Yes	Yes	No	No
A146	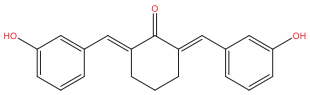	High	−3.95	Yes	No	No	No
HGV5	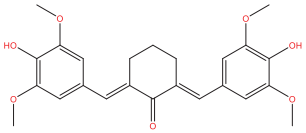	High	−3.10	No	No	No	No
HGV6	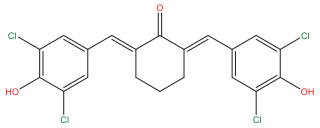	High	−4.89	Yes	No	No	No
THA102	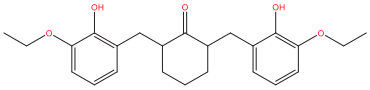	High	−3.91	Yes	Yes	No	No
THA103	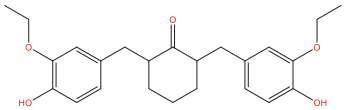	High	−3.91	Yes	Yes	No	No
THA104	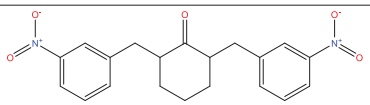	High	−4.75	No	No	No	No
THA108	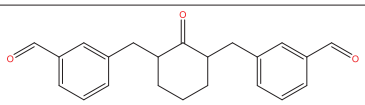	High	−4.31	Yes	Yes	No	No
THA111	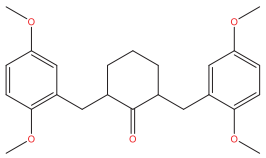	High	−4.13	Yes	Yes	No	No
THA113	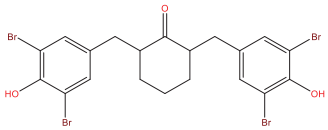	High	−5.76	Yes	No	No	No
THA129	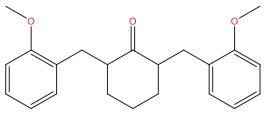	High	−4.76	Yes	Yes	No	No
THA146	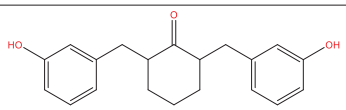	High	−3.95	Yes	No	No	No
THHGV5	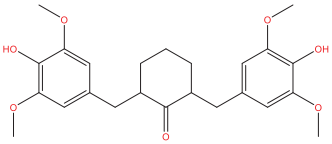	High	−3.10	No	No	No	No
THHGV6	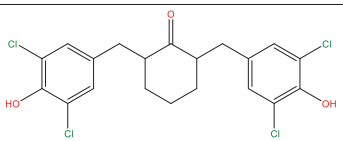	High	−4.89	Yes	No	No	No

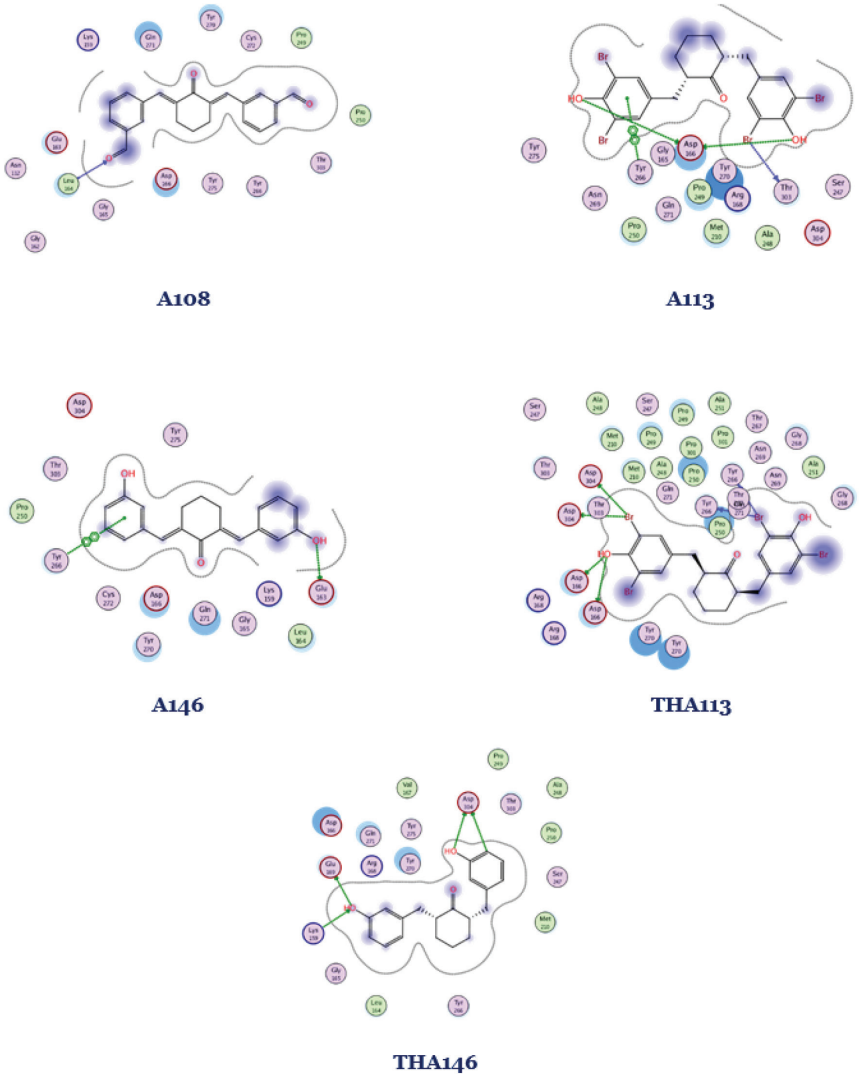

Figure 1. A graphical representation in two dimensions of the outcomes obtained from molecular docking investigations involving curcumin analogs and SARS-CoV-2 PLpro macromolecules.

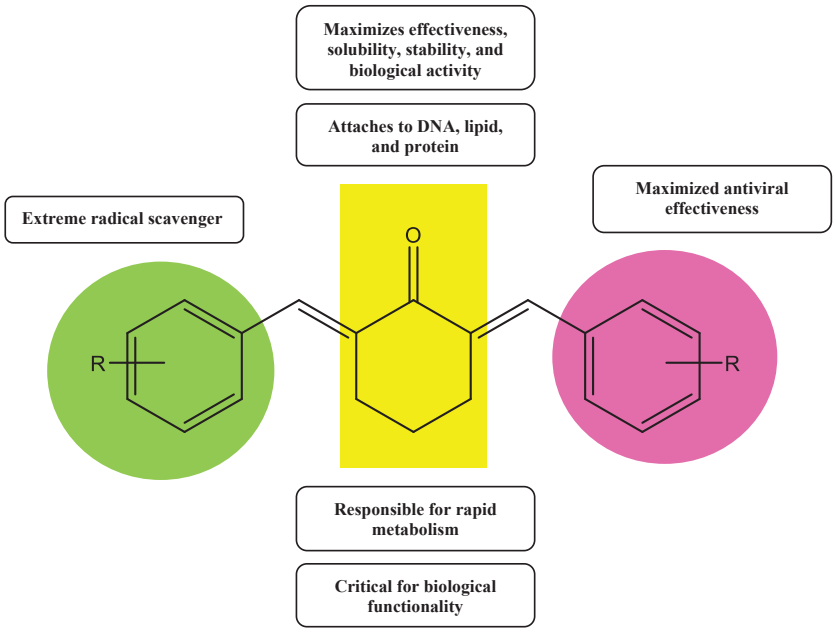

Figure 2. The chemical structure of curcumin along with its main pharmacophores and potential positions (Tomeh et al. 2019; Kaur et al. 2021).

PASS identification of curcumin analogs

The PASS server holds an extensive dataset for training, encompassing diverse bioactive compounds and their associations between structure and activity derived from a range of clinical and preclinical investigations. Using this dataset, the PASS server predicts the biological activity of chemical compounds (Islam et al. 2022). Examination of the biological activity of the refined compounds reveals that most derivatives of curcumin display inhibitory activity against 3C-like protease (Human coronavirus) and successfully clear the PASS biological activity screening (Table 3). The interpretation and application of PASS prediction outcomes are adaptable: only activities exceeding Pi are deemed plausible for a specific compound; if Pa surpasses 0.7, the likelihood of experimental activity discovery is considerable; for Pa values between 0.5 and <0.7, the prospect of experimental activity discovery is diminished, although the compound might diverge from established pharmaceutical agents; should Pa fall below 0.5, the probability of experimental activity discovery is minimal, yet the likelihood of encountering structurally novel chemical entities (NCEs) is heightened (Ramadhan et al. 2020).

Table 3. The primary 20 pertinent biological characteristics of the clarified curcumin analog compounds.

Compound Molecule	Molecular Structure	Possible Activity (Pa)	Possible Inactivity (Pi)	Biological Activity
A102	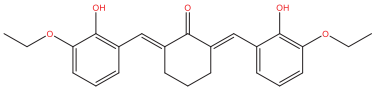	0.416	0,074	Antiviral (Rhinovirus)
		0.337	0.062	Antiviral (Adenovirus)
		0.364	0.143	Antiviral (Picornavirus)
		0.286	0.138	Simian immunodeficiency virus proteinase inhibitor
		0.212	0.147	3C-like protease (Human coronavirus) inhibitor
A103	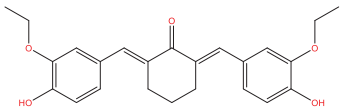	0.425	0.067	Antiviral (Rhinovirus)
		0.371	0.042	Antiviral (Adenovirus)
		0.330	0.183	Antiviral (Picornavirus)
		0.238	0.096	3C-like protease (Human coronavirus) inhibitor
		0.277	0.148	Simian immunodeficiency virus proteinase inhibitor
A104	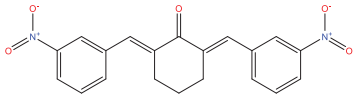	0.552	0.031	Antiviral (Picornavirus)
		0.488	0.023	Simian immunodeficiency virus proteinase inhibitor
		0.459	0.012	Antiviral (Adenovirus)
		0.396	0.004	3C-like protease (Human coronavirus) inhibitor
		0.195	0.166	Antiviral (Poxvirus)
A108	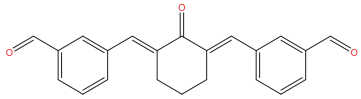	0.285	0.035	3C-like protease (Human coronavirus) inhibitor
		0.315	0.077	Antiviral (Adenovirus)
		0.326	0.099	Simian immunodeficiency virus proteinase inhibitor
		0.312	0.207	Antiviral (Picornavirus)
A111	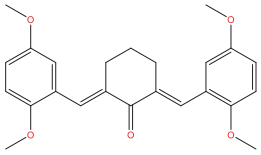	0.328	0.097	Simian immunodeficiency virus proteinase inhibitor
		0.272	0.047	3C-like protease (Human coronavirus) inhibitor
		0.285	0.102	Antiviral (Adenovirus)
		0.342	0.167	Antiviral (Picornavirus)
A113	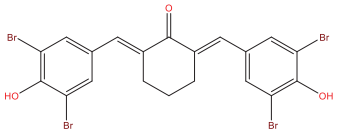	0.546	0.004	Antiviral (Adenovirus)
		0.284	0.037	3C-like protease (Human coronavirus) inhibitor
		0.285	0.138	Simian immunodeficiency virus proteinase inhibitor
		0.210	0.144	Antiviral (Poxvirus)
		0.279	0.263	Antiviral (Picornavirus)
A129	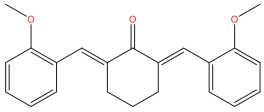	0.376	0.130	Antiviral (Picornavirus)
		0.376	0.130	Antiviral (Picornavirus)
		0.301	0.088	Antiviral (Adenovirus)
		0.316	0.107	Simian immunodeficiency virus proteinase inhibitor
A146	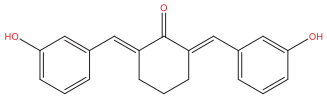	0.403	0.028	Antiviral (Adenovirus)
		0.320	0.015	3C-like protease (Human coronavirus) inhibitor
		0.349	0.081	Simian immunodeficiency virus proteinase inhibitor
		0.381	0.126	Antiviral (Picornavirus)
		0.194	0.168	Antiviral (Poxvirus)
HGV5	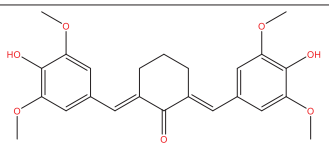	0.371	0.043	Antiviral (Adenovirus)
		0.289	0.032	3C-like protease (Human coronavirus) inhibitor
		0.322	0.193	Antiviral (Picornavirus)
		0.266	0.162	Simian immunodeficiency virus proteinase inhibitor
HGV6	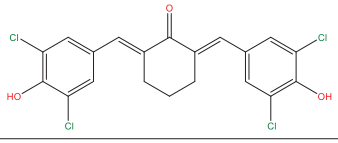	0.417	0.097	Antiviral (Picornavirus)
		0.344	0.057	Antiviral (Adenovirus)
		0.289	0.032	3C-like protease (Human coronavirus) inhibitor
		0.285	0.138	Simian immunodeficiency virus proteinase inhibitor
		0.187	0.180	Antiviral (Poxvirus)

Compound Molecule	Molecular Structure	Possible Activity (Pa)	Possible Inactivity (Pi)	Biological Activity
THA102	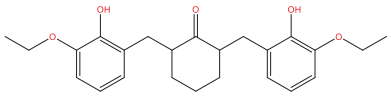	0.523	0.041	Antiviral (Picornavirus)
		0.431	0.062	Antiviral (Rhinovirus)
		0.274	0.113	Antiviral (Adenovirus)
		0.276	0.150	Simian immunodeficiency virus proteinase inhibitor
		0.229	0.111	3C-like protease (Human coronavirus) inhibitor
		0.214	0.138	Antiviral (Poxvirus)
THA103	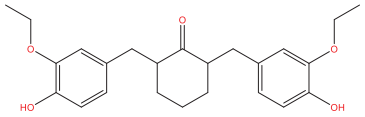	0.531	0.038	Antiviral (Picornavirus)
		0.439	0.056	Antiviral (Rhinovirus)
		0.247	0.081	3C-like protease (Human coronavirus) inhibitor
		0.261	0.127	Antiviral (Adenovirus)
		0.267	0.161	Simian immunodeficiency virus proteinase inhibitor
		0.201	0.157	Antiviral (Poxvirus)
THA104	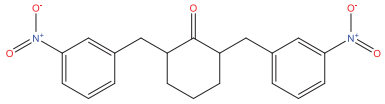	0.713	0.005	Antiviral (Picornavirus)
		0.476	0.026	Simian immunodeficiency virus proteinase inhibitor
		0.410	0.004	3C-like protease (Human coronavirus) inhibitor
		0.359	0.049	Antiviral (Adenovirus)
		0.227	0.120	Antiviral (Poxvirus)
		0.026	0.007	Protease (Human cytomegalovirus) inhibitor
THA108	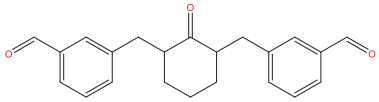	0.510	0.046	Antiviral (Picornavirus)
		0.294	0.028	3C-like protease (Human coronavirus) inhibitor
		0.315	0.108	Simian immunodeficiency virus proteinase inhibitor
		0.207	0.198	Antiviral (Adenovirus)
THA111	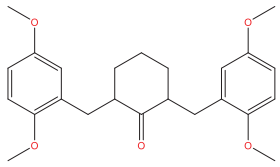	0.499	0.051	Antiviral (Picornavirus)
		0.289	0.032	3C-like protease (Human coronavirus) inhibitor
		0.317	0.106	Simian immunodeficiency virus proteinase inhibitor
		0.315	0.222	Antiviral (Rhinovirus)
		0.225	0.171	Antiviral (Adenovirus)
		0.188	0.179	Antiviral (Poxvirus)
THA113	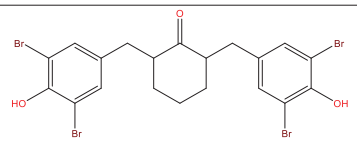	0.453	0.013	Antiviral (Adenovirus)
		0.467	0.066	Antiviral (Picornavirus)
		0.293	0.029	3C-like protease (Human coronavirus) inhibitor
		0.242	0.103	Antiviral (Poxvirus)
		0.275	0.150	Simian immunodeficiency virus proteinase inhibitor
THA129	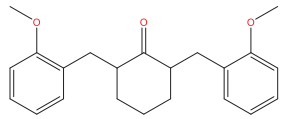	0.536	0.037	Antiviral (Picornavirus)
		0.298	0.026	3C-like protease (Human coronavirus) inhibitor
		0.306	0.116	Simian immunodeficiency virus proteinase inhibitor
		0.239	0.152	Antiviral (Adenovirus)
		0.203	0.154	Antiviral (Poxvirus)
		0.285	0.285	Antiviral (Rhinovirus)
THA146	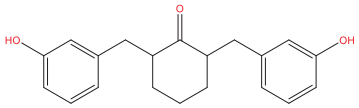	0.585	0.023	Antiviral (Picornavirus)
		0.330	0.012	3C-like protease (Human coronavirus) inhibitor
		0.338	0.088	Simian immunodeficiency virus proteinase inhibitor
		0.295	0.093	Antiviral (Adenovirus)
		0.226	0.122	Antiviral (Poxvirus)
THHGV5	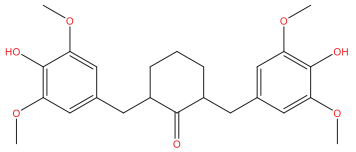	0.523	0.041	Antiviral (Picornavirus)
		0.298	0.026	3C-like protease (Human coronavirus) inhibitor
		0.260	0.128	Antiviral (Adenovirus)
		0.257	0.175	Simian immunodeficiency virus proteinase inhibitor
		0.203	0.154	Antiviral (Poxvirus)
		0.292	0.270	Antiviral (Rhinovirus)
THHGV6	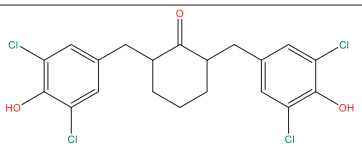	0.616	0.016	Antiviral (Picornavirus)
		0.298	0.026	3C-like protease (Human coronavirus) inhibitor
		0.275	0.150	Simian immunodeficiency virus proteinase inhibitor
		0.219	0.132	Antiviral (Poxvirus)
		0.233	0.160	Antiviral (Adenovirus)

Binding free energy MM-PBSA calculation

The subsequent step involves conducting molecular dynamics simulations between all curcumin-analog compounds and the SARS-CoV-2 PLpro macromolecules. Molecular dynamics simulations represent a computational technique employed to assess molecular behavior within biological systems (Muchtaridi et al. 2023). During molecular dynamics simulations, the positions and velocities of molecules are tracked over time using Newton's equations of motion and potential molecular interactions. Molecular dynamics simulations facilitate the examination of molecular dynamics under diverse conditions, including

temperature, pressure, and concentration (Pitaloka et al. 2021). They enable the assessment of processes such as compound-receptor interactions, chemical reactions, and alterations in molecular structure. Furthermore, molecular dynamics simulations allow for the investigation of changes in molecular structure and dynamics across varied environments, such as intracellular or extracellular environments.

The Molecular Mechanics Poisson-Boltzmann Surface Area (MM-PBSA) method is employed to assess the interaction energy between molecules and their surroundings within molecular dynamics simulations. This approach integrates principles from molecular mechanics and Poisson-Boltzmann theory to compute the interaction energy of molecules within their environment. MM-PBSA evaluates the interaction energy between molecules by employing molecular mechanics calculations to determine the potential energy within a molecule, which represents the energy required for forming its molecular structure (Kotni Meena 2015). Meanwhile, the Poisson-Boltzmann Surface Area (PBSA) component calculates the interaction energy between molecules and their environment, representing the energy needed to alter a molecule's shape from an ideal state to an observable form. MM-PBSA offers reliable estimations of molecular interaction energies within the systems under investigation, such as compound-receptor complexes.

Based on the results obtained from the MM-PBSA method for binding-free energy calculations, only five curcumin analog compounds demonstrated superior affinity and stability compared to the native ligands (GRL0617) during the 100 ns simulation in molecular dynamics interactions. Among these, A102, THA102, THA104, THA111, and THHGV6 exhibited the highest affinity stability, with binding free energy values of −108.975 kJ/mol, −108.931 kJ/mol, −108.975 kJ/mol, −106.188 kJ/mol, and −105.023 kJ/mol, respectively (Table 4). Generally, the primary contributors to energy in molecular dynamics simulations are kinetic and potential energies. Kinetic energy pertains to the energy associated with the motion of particles, while potential energy relates to their position within the system. Proper control of both kinetic and potential energies is essential in molecular dynamics simulations to maintain system stability in a thermodynamic state (Aulifa et al. 2024).

Table 4. The binding free energy MM-PBSA calculation of curcumin analogs with SARS-CoV-2 PLpro macromolecules.

Compound Molecule	ΔEvdw (kJ/mol)	ΔEele (kJ/mol)	ΔGPB (kJ/mol)	ΔGNP (kJ/mol)	ΔGBind (kJ/mol)
Native (GRL0617)	−149.05	−43.41	107.66	−16.17	−100.98
A102	−163.03	−32.83	103.36	−16.47	−108.98
A103	−104.99	−13.20	60.00	−12.46	−70.65
A104	−124.74	−21.12	100.84	−12.90	−57.91
A108	−115.35	−13.82	96.43	−12.88	−45.61
A111	−206.94	−30.14	171.81	−20.06	−85.33
A113	−146.69	−69.31	156.90	−13.61	−72.70
A129	−126.14	−4.07	75.85	−13.87	−68.24
A146	−81.52	−17.58	77.34	−9.68	−31.44
HGV5	−155.07	−40.02	125.77	−17.70	−87.03
HGV6	−137.38	−32.72	119.76	−16.32	−66.65
THA102	−180.07	−24.07	113.11	−17.89	−108.93
THA103	−107.48	−22.78	77.19	−12.62	−65.69
THA104	−163.03	−32.83	103.36	−16.47	−108.98
THA108	−116.88	−14.94	79.21	−13.56	−66.17
THA111	−170.04	−28.31	110.86	−18.70	−106.19
THA113	−107.50	−12.34	58.94	−11.15	−72.06
THA129	−112.04	−15.79	66.62	−12.70	−73.91
THA146	−129.58	−31.90	100.00	−14.88	−76.37
THHGV5	−151.65	−36.58	104.74	−15.67	−99.16
THHGV6	−155.60	−29.61	97.08	−16.89	−105.02

Information: ΔEvdw = van der Waals contribution, ΔEele = electrostatic contribution, ΔGPB = polar desolvation contribution, ΔGNP = non-polar desolvation contribution.

Interaction stability in molecular dynamics simulations

The purpose of trajectory visualization in molecular dynamics simulation is to enhance comprehension of particle behavior within the molecular system under investigation. In molecular dynamics simulations, particles, whether atoms or molecules, are discrete entities influenced by forces from other particles within the system. By visualizing particle trajectories, we can observe how particles interact and how alterations in simulation conditions, such as temperature or density, impact particle behavior. These visualizations aid in recognizing patterns and trends in particle motion, illustrating the correlation between particle movement and evolving system conditions, and portraying outcomes across various simulation scenarios.

Several factors can lead to the displacement of a compound from its binding site during molecular dynamics simulations. Primarily, the instability of the interaction potential energy between curcumin analog compounds and the binding sites of SARS-CoV-2 PLpro macromolecules plays a significant role. This potential energy, which governs the stability of the compound at the binding site, is determined by the molecular interaction potential employed in the simulation. Certain potential interactions promote the compound's stability at the binding site, while others may facilitate its movement away from it. Fig. 3 illustrates that the five curcumin analog compounds exhibiting the most favorable MM-PBSA binding-free energy demonstrate robust stability against the binding sites of SARS-CoV-2 PLpro macromolecules. These visual representations offer valuable insights into the atomic-level molecular interactions and provide guidance on potential modifications to optimize binding affinity and therapeutic effectiveness.

Furthermore, molecular dynamics simulations also consider the thermal transfer of atoms participating in interactions. If atoms involved in the interaction are sufficiently large during the heat transfer simulation, they may induce the compound to shift away from the binding site. To delve deeper into the molecular interactions during the 100 ns molecular dynamics simulations, Root Mean Square Deviation (RMSD) and Root Mean Square Fluctuation (RMSF) analyses were conducted. RMSD quantifies the average disparity between the protein's true conformation (derived from the crystal structure) and the conformation acquired from molecular dynamics

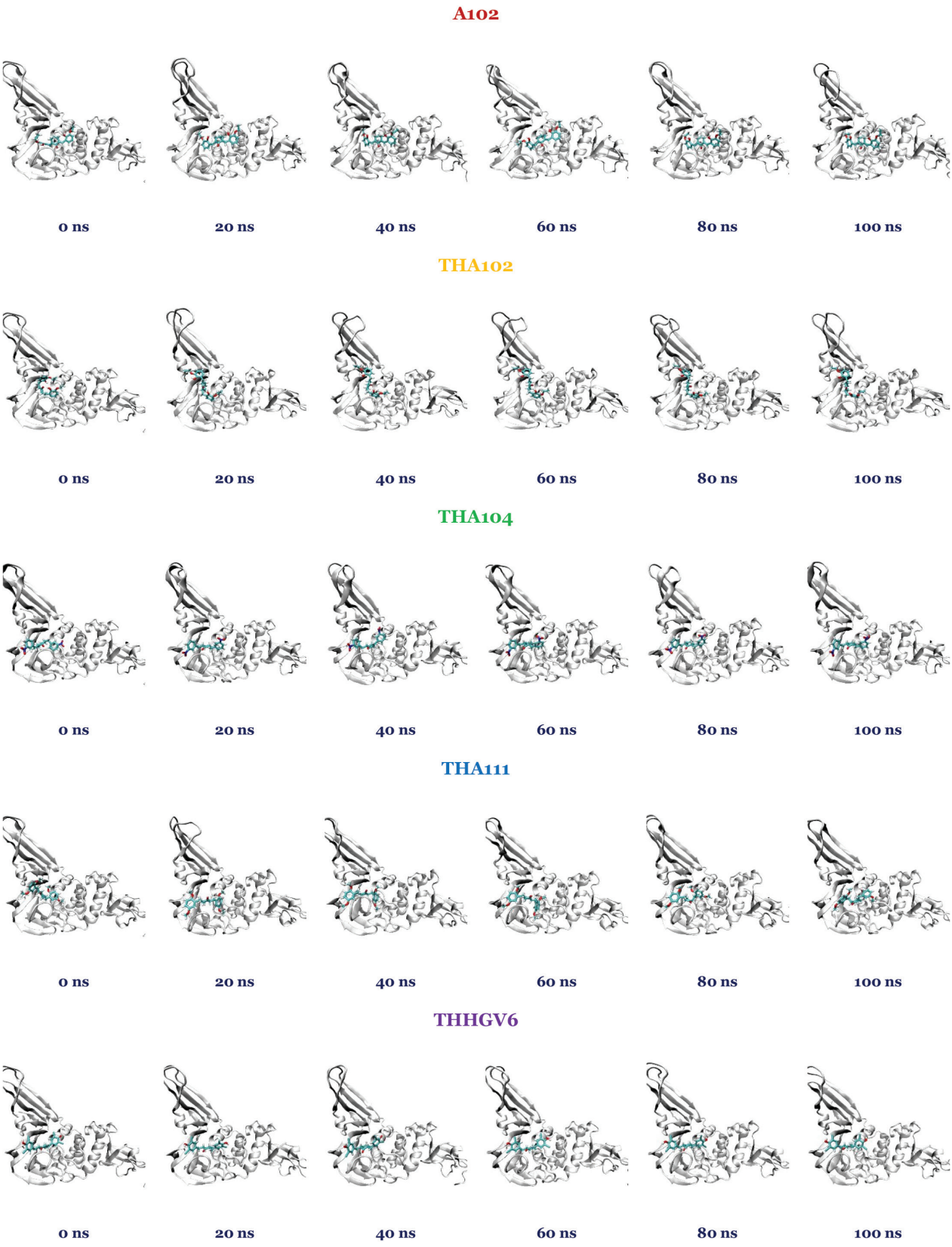

Figure 3. The three-dimensional depiction of molecular dynamics simulation outcomes involving curcumin analogs and SARS-CoV-2 PLpro macromolecules.

simulations. It is computed by measuring the mean distance between atoms in the two conformations. A low RMSD value suggests a close resemblance between the conformation from molecular dynamics simulations and the actual conformation. Conversely, RMSF assesses the average fluctuation of atomic positions in dynamic conformations obtained from molecular dynamics simulations. RMSF is determined by computing the average

distance of each atom from its mean position in the dynamic conformation. A high RMSF value indicates substantial atomic movement in the dynamic conformation obtained from molecular dynamics simulations (Hidayat and Fakih 2021).

The RMSD chart displayed in Fig. 4 illustrates notable fluctuations observed in the THA102 compound compared to the other four curcumin derivative compounds, with an average RMSD value of 2.74 Å. Conversely, the RMSF plot reveals that the THA111 compound induces fluctuations in various amino acid residues across different regions of the SARS-CoV-2 PLpro macromolecules, such as LYS192, HIE193, CYS194, VAL227, CYS228, GLY229, ARG230, ASP231, LYS281, and GLU282, averaging a RMSF value of 1.35 Å. RMSD and RMSF serve as metrics to assess alterations in protein structure during molecular dynamics simulations. Significant variations observed in the RMSD and RMSF graphs may stem from factors such as conformational shifts, protein-ligand interactions, thermal dynamics, and model precision.

Distribution of molecule movement during molecular dynamics simulations

Graphical examination of the radius of gyration (Rg) and solvent accessible surface area (SASA) is essential to validate the fluctuations observed in the results obtained from molecular dynamics simulations for each curcumin analog compound. Rg serves as a parameter to gauge the size and distribution of mass within molecules or molecular assemblies (Hikmawati et al. 2022). In the context of molecular dynamics simulations, Rg is utilized to assess the dimensions of the simulated protein, calculated as the average distance of each atom from the molecular geometry's center of mass. On the other hand, SASA quantifies the solvent-accessible surface area within a protein structure. Computed using the rolling ball algorithm, SASA determines the surface area accessible to atoms based on a sphere with a radius equivalent to that of an oxygen atom (Smith et al. 2015). During molecular dynamics simulations, SASA is instrumental in monitoring variations in the surface area accessible to solvent

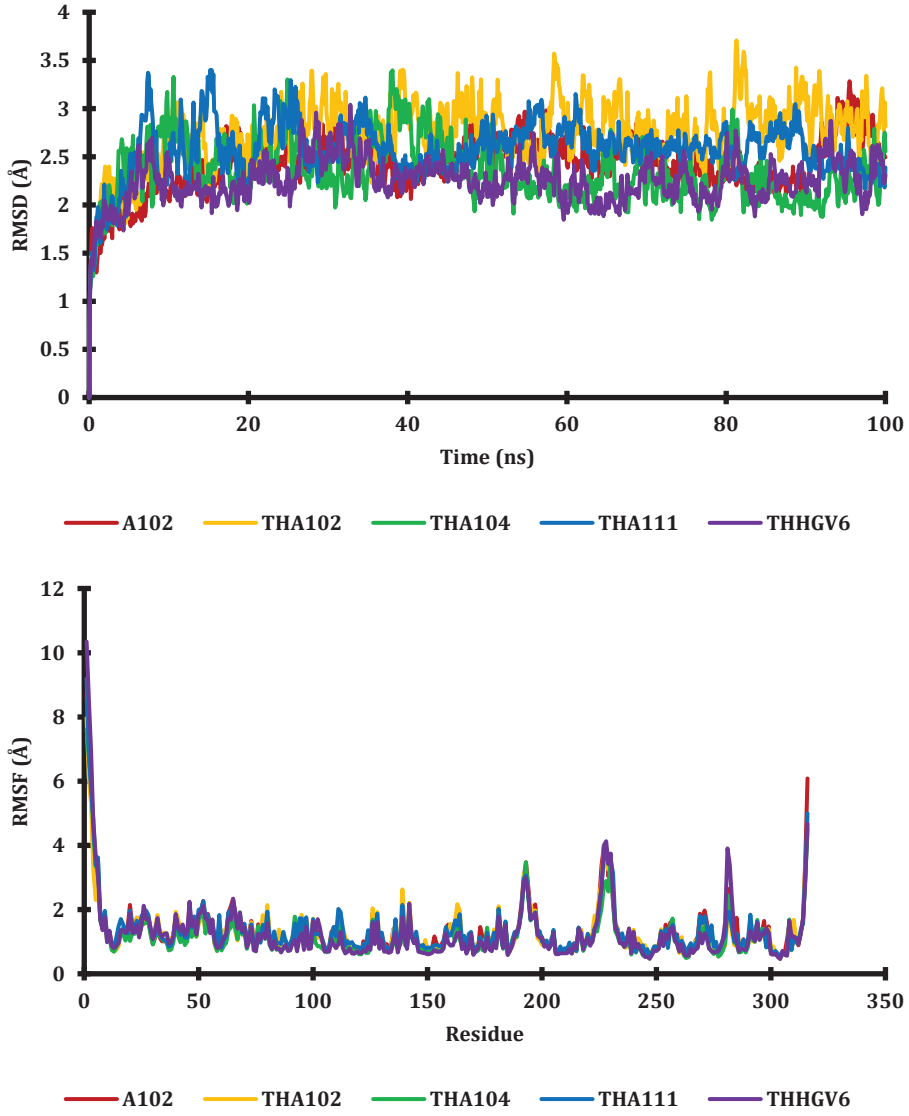

Figure 4. Visual representation of RMSD and RMSF data from molecular dynamics simulations depicting the behavior of curcumin analogs against SARS-CoV-2 PLpro macromolecules.

molecules. Additionally, SASA can delineate the nature of interactions within proteins, identifying hydrophobic interactions through decreased SASA and hydrophilic interactions through increased SASA.

Fig. 5 demonstrates that there are no substantial distinctions observed in the Rg and SASA graph visualizations for the five curcumin analog compounds. Rg and SASA serve as pivotal parameters in molecular dynamics simulations, facilitating the examination of molecule movement in solution. The Rg and SASA values for the five curcumin analogs exhibited negligible variance throughout the molecular dynamics simulation, indicating their akin physicochemical characteristics in solution. This uniformity may relate to the compound's solubility, stability, and potential impact on pharmacological efficacy. Nonetheless, it's essential to recognize that Rg and SASA values are merely a subset of parameters when assessing molecule properties in solution, necessitating a comprehensive analysis to discern disparities among the five curcumin analog compounds.

Atomic distribution in molecular dynamics simulations systems

The radial distribution function (RDF) serves as a metric utilized to assess the dispersion pattern of atoms or molecules within a system. In molecular dynamics simulations, RDF is employed to gauge the spatial arrangement of atoms within the simulated protein. This calculation involves dividing the mean distance between two distinct types of atoms by the average distance of identical atoms (Vijayakumar et al. 2022). The RDF analysis reveals that the THA102 compound exhibits dissimilar atomic distribution dynamics compared to other curcumin analog compounds throughout the 100 ns MD simulation. Variations in RDF can signify alterations in protein structure, potentially instigated by ligand interactions, environmental fluctuations, or thermal fluctuations. Additionally, RDF can discern the nature of protein interactions, indicating hydrophobic interactions when RDF decreases or hydrophilic interactions when RDF increases.

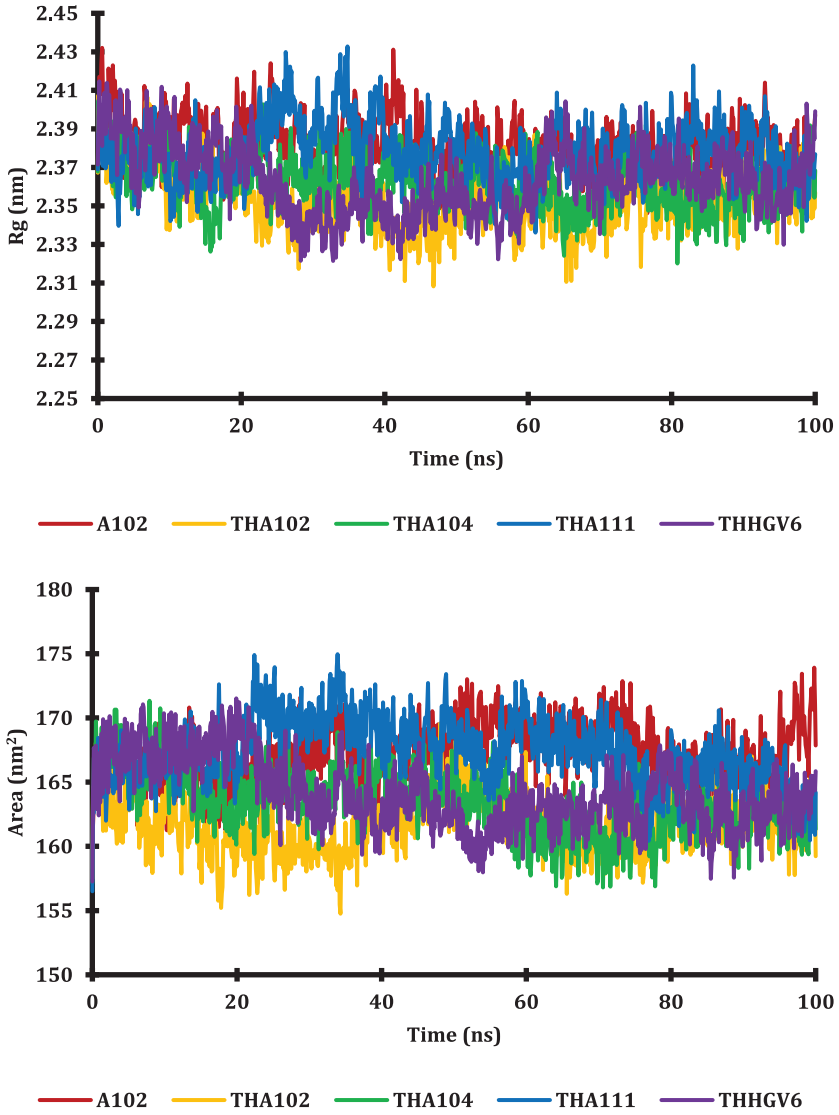

Figure 5. Visual representation of the molecular dynamics simulation outcomes for Rg and SASA is pivotal to illustrate the behavior of curcumin analogs in interaction with SARS-CoV-2 PLpro macromolecules.

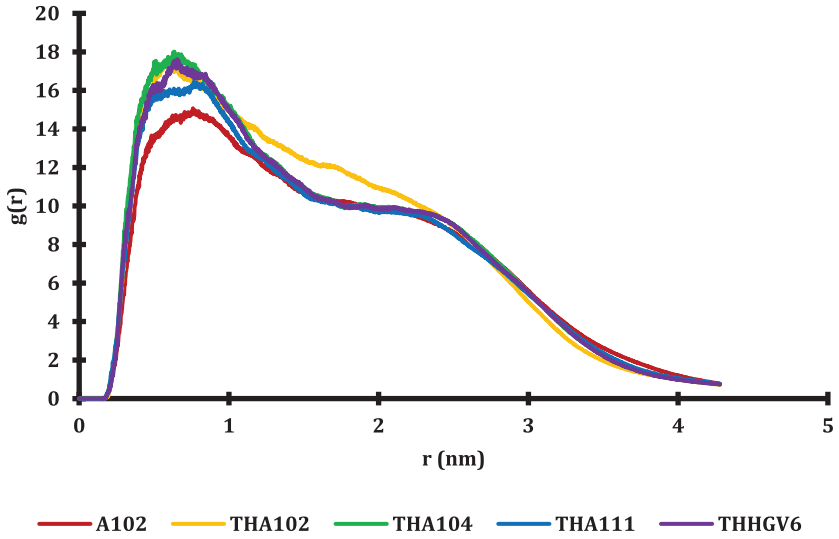

Figure 6. The graphical representation of RDF obtained from molecular dynamics simulations illustrates the outcome of the interactions between curcumin analogs and SARS-CoV-2 PLpro macromolecules.

Compound A102 exhibits a consistently stable and adaptable atomic dispersion throughout the simulations (Fig. 6). This suggests that these compounds foster robust atomic interactions, evenly spread around the SARS-CoV-2 PLpro macromolecules. This phenomenon may arise from the presence of stable and robust chemical bonds within compound A102, enhancing atomic interactions and facilitating flexible molecular movement. With its stable and adaptable atomic distribution, compound A102 is anticipated to exert a more pronounced biological impact, as it can engage more effectively with the target. Hence, RDF analysis aids in forecasting the therapeutic potential of compounds in pharmaceutical development.

Strength and geometry of hydrogen bonds in molecular dynamics simulations

Moreover, an assessment of the stability of the ligand-protein hydrogen bonds established during the molecular dynamics simulations was conducted. This entails scrutinizing the hydrogen bond dynamics derived from the simulations, encompassing the quantification of their quantity, strength, and configuration. This analysis involves parsing the atomic coordinate datasets generated from the simulations and aligning them with predefined geometric criteria for hydrogen bonding. The tally of hydrogen bonds formed serves as a metric to gauge system stability, with fluctuations indicating alterations in molecular conformation. Additionally, the vigor of the hydrogen bond is appraised through an examination of its potential energy, while its geometry is assessed by scrutinizing the distance and angle between the hydrogen and bonded atoms (Wibowo et al. 2022).

Based on the hydrogen bond occupancy data presented in Table 5, it is evident that compounds THA111 and THHGV6 maintain stable hydrogen bonds throughout the entire molecular dynamics simulations, as indicated by their total hydrogen bond occupancy percentages of 21.76% and 23.36%, respectively. In contrast, compounds A102, THA102, and THA104 exhibit lower hydrogen bond occupancy percentages, namely 11.28%, 6.29%, and 14.47%, respectively. The key amino acid residues in the SARS-CoV-2 PLpro macromolecules that predominantly form hydrogen bonds include LYS159, ASP166, GLU169, TYR266, TYR270, and GLN271. The high percentage of hydrogen bond occupancy observed in the molecular dynamics simulations signifies the stability of the hydrogen bonds formed, which is crucial as it can influence the physical and chemical properties of the simulated system.

Fig. 7 illustrates the consistent presence of stable hydrogen bonds between compounds THA111 and THHGV6 with SARS-CoV-2 PLpro macromolecules throughout the simulation. Compound THA111 displayed peak hydrogen bond occurrences at 38.7 ns, 77.5 ns, 91.1 ns, and 94.4 ns, while THHGV6 exhibited its highest hydrogen bond occurrences

Table 5. Percentage of hydrogen bonds formed by curcumin analogs with SARS-CoV-2 PLpro macromolecules.

Compound Molecule	Donor	Acceptor	Occupancy	Total Occupancy
A102	TYR266	A102	0.60%	11.28%
	LYS159	A102	0.10%	
	GLN271	A102	0.30%	
	GLN271	A102	0.90%	
	GLN271	A102	9.18%	
	A102	ASP166	0.20%	
THA102	THA102	ASP166	0.10%	6.29%
	GLN271	THA102	0.50%	
	TYR270	THA102	5.39%	
	GLN271	THA102	0.30%	
THA104	GLN271	THA104	14.37%	14.47%
	GLN271	THA104	0.10%	
THA111	GLN271	THA111	10.38%	21.76%
	GLN271	THA111	1.50%	
	GLN271	THA111	5.69%	
	TYR266	THA111	4.19%	
THHGV6	THHGV6	GLU169	1.20%	23.36%
	GLN271	THHGV6	22.16%	

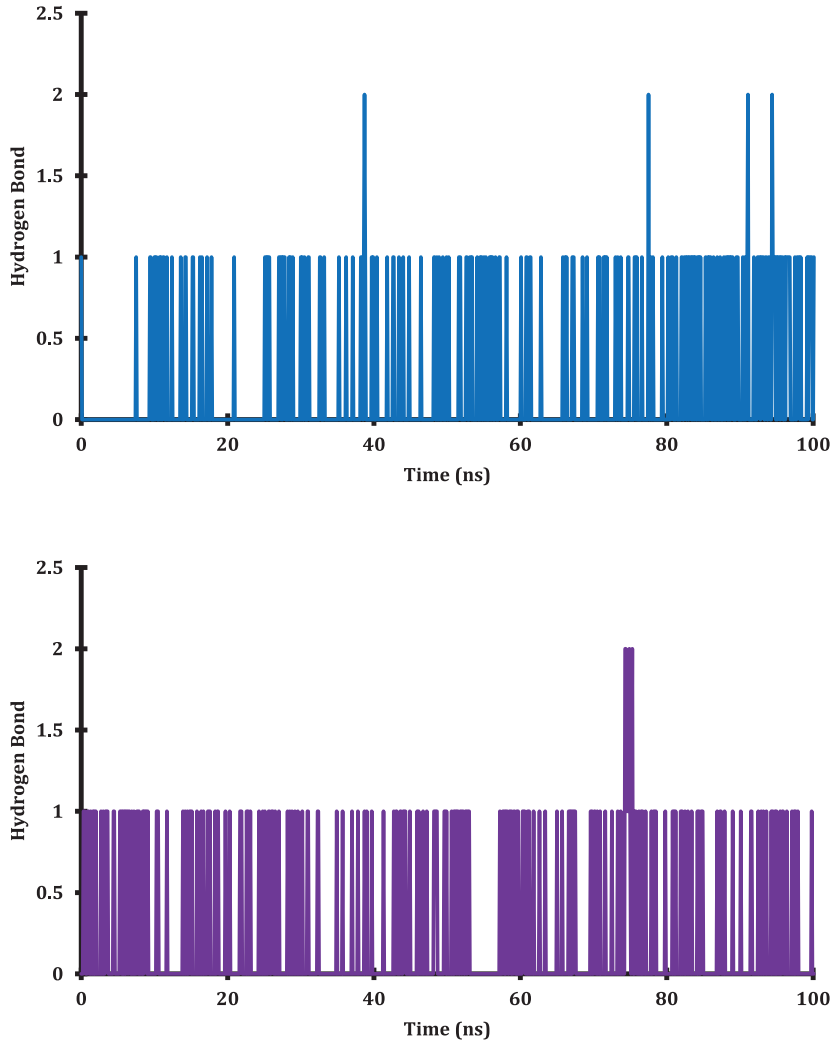

Figure 7. Visual representations of the outcomes of molecular dynamics simulations regarding hydrogen bonds formed between THA111 (depicted in blue) and THHGV6 (shown in purple) with SARS-CoV-2 PLpro macromolecules.

at 74.3 ns, 74.4 ns, 74.9 ns, and 75.3 ns. A significant number of hydrogen bonds observed during molecular dynamics simulations suggests that both THA111 and THHGV6 possess robust and enduring molecular structures. This observation implies that the curcumin analog compounds potentially engage in numerous hydrogen bonding interactions, forming a dense or interconnected network.

Conclusions

The simulations indicate that overall, curcumin analog compounds exhibit favorable binding to SARS-CoV-2 papain-like protease (PLpro) macromolecules. However, THA111 and THHGV6 compounds demonstrated superior stability and affinity for SARS-CoV-2 PLpro macromolecules in both molecular dynamics simulations and MM-PBSA binding-free energy calculations. Consequently, these two compounds emerge as promising therapeutic candidates for combating COVID-19.

Acknowledgments

Author thanks the Curcumin Research Centre, Faculty of Pharmacy, Universitas Gadjah Mada, for providing the database of curcumin analog compounds used in this study.

This research received no external funding.

References

Abduljalil JM, Abduljalil BM (2020) Epidemiology, genome, and clinical features of the pandemic SARS-CoV-2: a recent view. New Microbes and New Infections 35: 100672. https://doi.org/10.1016/j.nmni.2020.100672

Abraham M, Hess B, Spoel D van der, Lindahl E (2015) The GROMACS development team, GROMACS user manual. Version 5.0.7.

Adamczak A, Ożarowski M, Karpiński TM (2020) Curcumin, a natural antimicrobial agent with strain-specific activity. Pharmaceuticals 13(7): 153. https://doi.org/10.3390/ph13070153

Angamuthu D, Purushothaman I, Kothandan S, Swaminathan R (2019) Antiviral study on *Punica granatum* L., *Momordica charantia* L.,

Andrographis paniculata Nees, and *Melia azedarach* L., to Human Herpes Virus-3. European Journal of Integrative Medicine 28(4): 98–108. https://doi.org/10.1016/j.eujim.2019.04.008

Aragones JL, Noya EG, Valeriani C, Vega C (2013) Free energy calculations for molecular solids using GROMACS. Journal of Chemical Physics 139: 034104. https://doi.org/10.1063/1.4812362

Ariyanto EF, Shalannandia WA, Lantika UA, Fakih TM, Ramadhan DSF, Gumilar AN, Permana FK, Rahmah AN, Atik N, Khairani AF (2023) Anthocyanin-containing purple sweet potato (*Ipomoea batatas* L.) Synbiotic Yogurt Inhibited 3T3-L1 Adipogenesis by Suppressing White Adipocyte-Specific Genes. Journal of Experimental Pharmacology 15: 217–230. https://doi.org/10.2147/JEP.S405433

Aulifa DL, Al Shofwan AA, Megantara S, Fakih TM, Budiman A (2024) Elucidation of Molecular Interactions Between Drug–Polymer in Amorphous Solid Dispersion by a Computational Approach Using Molecular Dynamics Simulations. Advances and Applications in Bioinformatics and Chemistry 17: 1–19. https://doi.org/10.2147/AABC.S441628

Bianchi E, Pessi A (2002) Inhibiting viral proteases: Challenges and opportunities. Biopolymers 66(2): 101–114. https://doi.org/10.1002/bip.10230

BIOVIA (2017) Dassault Systèmes BIOVIA, Discovery Studio Modeling Environment, Release 2017. Dassault Systèmes San Diego.

Brown T (2014) ChemDraw. The Science Teacher 81. https://doi.org/10.12968/prtu.2014.1.37.65

Cheung CKM, Law MF, Lui GCY, Wong SH (2021) Coronavirus Disease 2019 (COVID-19): A Haematologist's Perspective. Acta Haematologica 144(1): 10–23. https://doi.org/10.1159/000510178

Daina A, Michielin O, Zoete V (2017) SwissADME: A free web tool to evaluate pharmacokinetics, drug-likeness and medicinal chemistry friendliness of small molecules. Scientific Reports 7: 42717. https://doi.org/10.1038/srep42717

Das S, Sarmah S, Lyndem S, Singha Roy A (2021) An investigation into the identification of potential inhibitors of SARS-CoV-2 main protease using molecular docking study. Journal of Biomolecular Structure and Dynamics 39(9): 3347–3357. https://doi.org/10.1080/07391102.2020.1763201

Deshmukh TR, Krishna VS, Sriram D, Sangshetti JN, Shingate BB (2020) Synthesis and bioevaluation of α,α'-bis(1H-1,2,3-triazol-5-ylmethylene) ketones. Chemical Papers 74(3): 809–820. https://doi.org/10.1007/s11696-019-00908-5

Fakih TM (2023) Molecularly imprinted polymer-based sensors for identification volatile compounds in pharmaceutical products: in silico rational design. Journal of Biomolecular Structure and Dynamics 1–11. https://doi.org/10.1080/07391102.2023.2252090

Fernández-Castañeda A, Lu P, Geraghty AC, Song E, Lee MH, Wood J, O'Dea MR, Dutton S, Shamardani K, Nwangwu K, Mancusi R, Yalçın B, Taylor KR, Acosta-Alvarez L, Malacon K, Keough MB, Ni L, Woo PJ, Contreras-Esquivel D, Toland AMS, Gehlhausen JR, Klein J, Takahashi T, Silva J, Israelow B, Lucas C, Mao T, Peña-Hernández MA, Tabachnikova A, Homer RJ, Tabacof L, Tosto-Mancuso J, Breyman E, Kontorovich A, McCarthy D, Quezado M, Vogel H, Hefti MM, Perl DP, Liddelow S, Folkerth R, Putrino D, Nath A, Iwasaki A, Monje M (2022) Mild respiratory COVID can cause multi-lineage neural cell and myelin dysregulation. Cell 185(14): 2452–2468. https://doi.org/10.1016/j.cell.2022.06.008

Forli W, Halliday S, Belew R, Olson A (2012) AutoDock Version 4.2. Citeseer.

Frisch MJ, Trucks GW, Schlegel HB, Scuseria GE, Robb MA, Cheeseman JR, Scalmani G, Barone V, Mennucci B, Petersson GA, Nakatsuji H, Caricato M, Li X, Hratchian HP, Izmaylov AF, Bloino J, Zheng G, Sonnenberg JL, Hada M, Ehara M, Toyota K, Fukuda R, Hasegawa J, Ishida M, Nakajima T, Honda Y, Kitao O, Nakai H, Vreven T, Montgomery JAJ, Peralta PE, Ogliaro F, Bearpark M, Heyd JJ, Brothers E, Kudin KN, Staroverov VN, Kobayashi R, Normand J, Raghavachari K, Rendell A, Burant JC, Iyengar SS, Tomasi J, Cossi M, Rega N, Millam NJ, Klene M, Knox JE, Cross JB, Bakken V, Adamo C, Jaramillo J, Gomperts R, Stratmann RE, Yazyev O, Austin AJ, Cammi R, Pomelli C, Ochterski JW, Martin RL, Morokuma K, Zakrzewski VG, Voth GA, Salvador P, Dannenberg JJ, Dapprich S, Daniels AD, Farkas Ö, Ortiz J V, Cioslowski J, Fox DJ (2009) Gaussian 09, revision C.01; Gaussian Inc.: Wallingford, CT.

Gil RM, Marcelin JR, Zuniga-Blanco B, Marquez C, Mathew T, Piggott DA (2020) COVID-19 pandemic: Disparate health impact on the hispanic/latinx population in the United States. Journal of Infectious Diseases 222(10): 1592–1595. https://doi.org/10.1093/infdis/jiaa474

Hidayat AF, Fakih TM (2021) Self-assembly of black cumin oil-based nanoemulsion on various surfactants: A molecular dynamics study. Makara Journal of Science 25(4): 258–264. https://doi.org/10.7454/mss.v25i4.1267

Hikmawati D, Fakih TM, Sutedja E, Dwiyana RF, atik N, Ramadhan DSF (2022) Pharmacophore-guided virtual screening and dynamic simulation of Kallikrein-5 inhibitor: Discovery of potential molecules for rosacea therapy. Informatics in Medicine Unlocked 28: 100844. https://doi.org/10.1016/j.imu.2022.100844

Hulce KR, Jaishankar P, Lee GM, Bohn MF, Connelly EJ, Wucherer K, Ongpipattanakul C, Volk RF, Chuo SW, Arkin MR, Renslo AR, Craik CS (2022) Inhibiting a dynamic viral protease by targeting a non-catalytic cysteine. Cell Chemical Biology 29(5): 785–798. https://doi.org/10.1016/j.chembiol.2022.03.007

Islam S, Hosen MA, Ahmad S, ul Qamar MT, Dey S, Hasan I, Fujii Y, Ozeki Y, Kawsar SMA (2022) Synthesis, antimicrobial, anticancer activities, PASS prediction, molecular docking, molecular dynamics and pharmacokinetic studies of designed methyl α-D-glucopyranoside esters. Journal of Molecular Structure 1260: 132761. https://doi.org/10.1016/j.molstruc.2022.132761

Kaur G, Kaur M, Bansal M (2021) New insights of structural activity relationship of curcumin and correlating their efficacy in anticancer studies with some other similar molecules. American Journal of Cancer Research 11(8): 3755–3765.

Kong A, Oh J-E, Lam T (2021) Face mask effects during COVID-19: perspectives of managers, practitioners and customers in the hotel industry. International Hospitality Review 35(2): 195–207. https://doi.org/10.1108/IHR-07-2020-0025

Kotha RR, Luthria DL (2019) Curcumin: Biological, pharmaceutical, nutraceutical, and analytical aspects. Molecules 24(16): 2930. https://doi.org/10.3390/molecules24162930

Kotni Meena NC (2015) QM/MM Docking Strategy and Prime/MM-GBSA Calculation of Celecoxib Analogues as N-myristoyltransferase Inhibitors. Virology & Mycology 4(1): 1–8. https://doi.org/10.4172/2161-0517.1000141

Kumar N, Kaur K, Bedi PMS (2023) Hybridization of molecular docking studies with machine learning based QSAR model for prediction of xanthine oxidase activity. Computational and Theoretical Chemistry 1227: 114262. https://doi.org/10.1016/j.comptc.2023.114262

Li D, Luan J, Zhang L (2021) Molecular docking of potential SARS-CoV-2 papain-like protease inhibitors. Biochemical and Biophysical Research Communications 538: 72–79. https://doi.org/10.1016/j.bbrc.2020.11.083

Linda Laksmiani NP, Febryana Larasanty LP, Jaya Santika AAG, Andika Prayoga PA, Kharisma Dewi AAI, Kristiara Dewi NPA (2020) Active compounds activity from the medicinal plants against SARS-CoV-2 using in silico assay. Biomedical and Pharmacology Journal 13(2): 873–881. https://doi.org/10.13005/bpj/1953

Lohidashan K, Rajan M, Ganesh A, Paul M, Jerin J (2018) Pass and Swiss ADME collaborated in silico docking approach to the synthesis of certain pyrazoline spacer compounds for dihydrofolate reductase inhibition and antimalarial activity. Bangladesh Journal of Pharmacology 13: 23–29. https://doi.org/10.3329/bjp.v13i1.33625

Marín-Palma D, Tabares-Guevara JH, Zapata-Cardona MI, Flórez-álvarez L, Yepes LM, Rugeles MT, Zapata-Builes W, Hernandez JC, Taborda NA (2021) Curcumin inhibits in vitro sars-cov-2 infection in vero e6 cells through multiple antiviral mechanisms. Molecules 26(22): 6900. https://doi.org/10.3390/molecules26226900

Mishra A, Mulpuru V, Mishra N (2022) Exploring the mechanism of action of podophyllotoxin derivatives through molecular docking, molecular dynamics simulation and MM/PBSA studies. Journal of Biomolecular Structure and Dynamics 41(18): 8856–8865. https://doi.org/10.1080/07391102.2022.2138549

Misran MRI Bin, Nunotani N, Tamura S, Imanaka N (2020) Enhancement of bromide ion conductivity in lanthanum oxybromide based solids by doping divalent zinc ion with high electronegativity. Journal of Asian Ceramic Societies 8(3): 925–929. https://doi.org/10.1080/21870764.2020.1793877

Mohamed Thamby BF, Santhi VM, Ramalingam A (2023) Quantum chemical and experimental studies on the extraction of acid blue 80 and acid red 1 from their aquatic environment using tetrabutylammonium bromide based deep eutectic solvents. Journal of Dispersion Science and Technology 44(9): 1778–1787. https://doi.org/10.1080/01932691.2023.2195931

Muchtaridi M, Triwahyuningtyas D, Muhammad Fakih T, Megantara S, Choi SB (2023) Mechanistic insight of α-mangostin encapsulation in 2-hydroxypropyl-β-cyclodextrin for solubility enhancement. Journal of Biomolecular Structure and Dynamics 42(6): 3223–3232. https://doi.org/10.1080/07391102.2023.2214237

Nocito MC, De Luca A, Prestia F, Avena P, La Padula D, Zavaglia L, Sirianni R, Casaburi I, Puoci F, Chimento A, Pezzi V (2021) Antitumoral activities of curcumin and recent advances to improve its oral bioavailability. Biomedicines 9(10): 1476. https://doi.org/10.3390/biomedicines9101476

Nurisyah, Ramadhan DSF, Dewi R, asikin A, Daswi DR, Adam A, Chaerunnimah, Sunarto, Rafika, Artati, Fakih TM (2024) Targeting EGFR allosteric site with marine-natural products of *Clathria* sp.: A computational approach. Current Research in Structural Biology 7: 100125. https://doi.org/10.1016/j.crstbi.2024.100125

Osipiuk J, Azizi SA, Dvorkin S, Endres M, Jedrzejczak R, Jones KA, Kang S, Kathayat RS, Kim Y, Lisnyak VG, Maki SL, Nicolaescu V, Taylor CA, Tesar C, Zhang YA, Zhou Z, Randall G, Michalska K, Snyder SA, Dickinson BC, Joachimiak A (2021) Structure of papain-like protease from SARS-CoV-2 and its complexes with non-covalent inhibitors. Nature Communications 12(1): 743. https://doi.org/10.1038/s41467-021-21060-3

Pires DEV, Blundell TL, Ascher DB (2015) pkCSM: Predicting small-molecule pharmacokinetic and toxicity properties using graph-based signatures. Journal of Medicinal Chemistry 58(9): 4066–4072. https://doi.org/10.1021/acs.jmedchem.5b00104

Pitaloka DAE, Ramadhan DSF, Arfan, Chaidir L, Fakih TM (2021) Docking-based virtual screening and molecular dynamics simulations of quercetin analogs as enoyl-acyl carrier protein reductase (Inha) inhibitors of mycobacterium tuberculosis. Scientia Pharmaceutica 89(2): 20. https://doi.org/10.3390/scipharm89020020

Ramadhan DSF, Fakih TM, Arfan A (2020) Activity Prediction of Bioactive Compounds Contained in Etlingera elatior Against the SARS-CoV-2 Main Protease: An In Silico Approach. Borneo Journal of Pharmacy 3(4): 235–242. https://doi.org/10.33084/bjop.v3i4.1634

Ramadhan DSF, Siharis F, Abdurrahman S, Isrul M, Fakih TM (2022) In silico analysis of marine natural product from sponge (*Clathria* Sp.) for their activity as inhibitor of SARS-CoV-2 Main Protease. Journal of Biomolecular Structure and Dynamics 40(22): 11526–11532. https://doi.org/10.1080/07391102.2021.1959405

Ratia K, Pegan S, Takayama J, Sleeman K, Coughlin M, Baliji S, Chaudhuri R, Fu W, Prabhakar BS, Johnson ME, Baker SC, Ghosh AK, Mesecar AD (2008) A noncovalent class of papain-like protease/deubiquitinase inhibitors blocks SARS virus replication. Proceedings of the National Academy of Sciences of the United States of America 105(42): 16119–16124. https://doi.org/10.1073/pnas.0805240105

Sencanski M, Perovic V, Milicevic J, Todorovic T, Prodanovic R, Veljkovic V, Paessler S, Glisic S (2022) Identification of SARS-CoV-2 Papain-like Protease (PLpro) Inhibitors Using Combined Computational Approach. ChemistryOpen 11(2): e202100248. https://doi.org/10.1002/open.202100248

Shah V, Bhaliya J, Patel GM (2022) In silico docking and ADME study of deketene curcumin derivatives (DKC) as an aromatase inhibitor or antagonist to the estrogen-alpha positive receptor (Erα+): potent application of breast cancer. Structural Chemistry 33(2): 571–600. https://doi.org/10.1007/s11224-021-01871-2

Smith MD, Rao JS, Segelken E, Cruz L (2015) Force-Field Induced Bias in the Structure of Aβ21-30: A Comparison of OPLS, AMBER, CHARMM, and GROMOS Force Fields. Journal of Chemical Information and Modeling 55(12): 2587–2595. https://doi.org/10.1021/acs.jcim.5b00308

Sun D, Zhuang X, Xiang X, Liu Y, Zhang S, Liu C, Barnes S, Grizzle W, Miller D, Zhang HG (2010) A novel nanoparticle drug delivery system: The anti-inflammatory activity of curcumin is enhanced when encapsulated in exosomes. Molecular Therapy 18(9): 1606–1614. https://doi.org/10.1038/mt.2010.105

Tan H, Hu Y, Jadhav P, Tan B, Wang J (2022) Progress and Challenges in Targeting the SARS-CoV-2 Papain-like Protease. Journal of Medicinal Chemistry 65(11): 7561–7580. https://doi.org/10.1021/acs.jmedchem.2c00303

Tomeh MA, Hadianamrei R, Zhao X (2019) A review of curcumin and its derivatives as anticancer agents. International Journal of Molecular Sciences 20(5): 1033. https://doi.org/10.3390/ijms20051033

Urošević M, Nikolić L, Gajić I, Nikolić V, Dinić A, Miljković V (2022) Curcumin: Biological Activities and Modern Pharmaceutical Forms. Antibiotics 11(2): 135. https://doi.org/10.3390/antibiotics11020135

Vijayakumar SD, Zakaria J, Ridzuan N (2022) Molecular dynamics approach on intermolecular interaction between n-icosane and gemini surfactant assisted nanoparticles. Petroleum Research 7(3): 366–371. https://doi.org/10.1016/j.ptlrs.2021.12.001

van Vliet VJE, Huynh N, Palà J, Patel A, Singer A, Slater C, Chung J, van Huizen M, Teyra J, Miersch S, Luu GK, Ye W, Sharma N, Ganaie SS, Russell R, Chen C, Maynard M, Amarasinghe GK, Mark BL, Kikkert M, Sidhu SS (2022) Ubiquitin variants potently inhibit SARS-CoV-2

PLpro and viral replication via a novel site distal to the protease active site. PLOS Pathogens 18(12): e1011065. https://doi.org/10.1371/journal.ppat.1011065

Wang C, Greene D, Xiao L, Qi R, Luo R (2018) Recent developments and applications of the MMPBSA method. Frontiers in Molecular Biosciences 4: 87. https://doi.org/10.3389/fmolb.2017.00087

Wibowo ZK, Ramadhani AS, Rachman MA, Khaerunnisa S (2022) In Silico Analysis of Potential Nicotine Addiction Treatment by Cinnamomum verum Phytochemicals against nAChRα3 and nAChRα7. International Journal of Scientific Advances 3(1): 42–48. https://doi.org/10.51542/ijscia.v3i1.5

Wurtzer S, Marechal V, Mouchel JM, Maday Y, Teyssou R, Richard E, Almayrac JL, Moulin L (2020) Evaluation of lockdown effect on SARS-CoV-2 dynamics through viral genome quantification in waste water, Greater Paris, France, 5 March to 23 April 2020. Eurosurveillance 25(50): 2000776. https://doi.org/10.2807/1560-7917.ES.2020.25.50.2000776

Yapasert R, Khaw-On P, Banjerdpongchai R (2021) Coronavirus infection-associated cell death signaling and potential therapeutic targets. Molecules 26(24): 7459. https://doi.org/10.3390/molecules26247459

Zhao G, Liu X, Wang S, Bai Z, Zhang S, Wang Y, Yu H, Xu X (2022) Hydrogen bonding penalty used for virtual screening to discover potent inhibitors for Papain-Like cysteine proteases of SARS-CoV-2. Chemical Biology and Drug Design 100(4): 502–514. https://doi.org/10.1111/cbdd.14115

Zorofchian Moghadamtousi S, Abdul Kadir H, Hassandarvish P, Tajik H, Abubakar S, Zandi K (2014) A review on antibacterial, antiviral, and antifungal activity of curcumin. BioMed Research International 2014: 186864. https://doi.org/10.1155/2014/186864

Zupin L, Fontana F, Clemente L, Borelli V, Ricci G, Ruscio M, Crovella S (2022) Optimization of Anti-SARS-CoV-2 Treatments Based on Curcumin, Used Alone or Employed as a Photosensitizer. Viruses 14(10): 2132. https://doi.org/10.3390/v14102132